Inorganic Chemistry

ARTICLE

pubs.acs.org/IC

"A" Cation Polarity Control in $ACuTe_2O_7$ (A = Sr^{2+}, Ba^{2+}, or Pb^{2+})

Jeongho Yeon,[†] Sang-Hwan Kim,[†] Michael A. Hayward,[‡] and P. Shiv Halasyamani*[,†]

[†]Department of Chemistry, University of Houston, 136 Fleming Building, Houston, Texas 77204-5003, United States

[‡]Inorganic Chemistry Laboratory, University of Oxford, South Parks Road, Oxford, OX1 3QR, United Kingdom

Supporting Information

ABSTRACT: The synthesis and characterization of $ACuTe_2O_7$ (A = Sr^{2+}, Ba^{2+}, or Pb^{2+}) have been carried out. Interestingly, $SrCuTe_2O_7$ and $PbCuTe_2O_7$ are centrosymmetric and isostructural, whereas $BaCuTe_2O_7$ is noncentrosymmetric and polar. All of the materials contain $[CuTe_2O_7]^{2-}$ layers stacked along the *b*-axis direction that are separated by the "A" cations. The layers are composed of corner-shared CuO_5, TeO_6, and TeO_4 polyhedra. The influence of the "A" cation on the polarity is described by bond valence concepts, including the bond strain index and global instability index. Infrared, UV−vis, thermogravimetric, differential thermal analysis, and magnetic measurements were performed on all three materials. For $BaCuTe_2O_7$, second-harmonic generation (SHG), piezoelectric, and polarization measurements were performed. A moderate SHG efficiency of approximately 70 × α-SiO_2 was measured. In addition, we determined that $BaCuTe_2O_7$ is not ferroelectric; that is, the macroscopic polarization is not reversible. For $BaCuTe_2O_7$, a pyroelectric coefficient of −9.5 $\mu C/m^2 \cdot K$ at 90 °C and a piezoelectric charge coefficient of 49 pm/V were determined. Crystal data are the following: $SrCuTe_2O_7$, orthorhombic, space group *Pbcm* (No. 57), a = 7.1464(7) Å, b = 15.0609(15) Å, c = 5.4380(5) Å, V = 585.30(10) $Å^3$, and Z = 4; $PbCuTe_2O_7$, orthorhombic, space group *Pbcm* (No. 57), a = 7.2033(5) Å, b = 15.0468(10) Å, c = 5.4691(4) Å, V = 592.78(7) $Å^3$, and Z = 4.

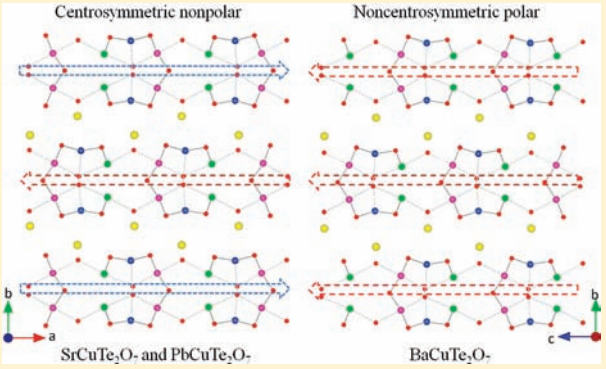

INTRODUCTION

Noncentrosymmetric (NCS) polar materials are of current interest attributable to their technologically relevant functional properties, for example, second-harmonic generation, ferroelectricity, pyroelectricity, etc.[1−5] From a crystallographic standpoint, a material is considered polar if it is found in 1 of 10 polar crystal classes.[6] Specific polar directions for each of these crystal classes have been defined.[6] Two functional properties associated with polarity and polar materials are ferroelectricity and pyroelectricity.[3] With ferroelectricity, the observed macroscopic polarization may be switched, or reversed, in the presence of an external electric field,[1] whereas for pyroelectricity, this polarization reversal does not necessarily occur.[3] Thus, polar materials may be ferroelectric, pyroelectric or nonferroelectric pyroelectric. With respect to new materials, a number of strategies have been published on the design of new polar compounds.[7−25] We have focused on synthesizing new materials containing cations susceptible to second-order Jahn−Teller distortions,[26−32] octahedrally coordinated d^0 transition-metal cations (Ti^{4+}, Nb^{5+}, W^{6+}, etc.) and lone-pair cations (Se^{4+}, Te^{4+}, I^{5+}, etc.). With both groups, the cation is in a locally asymmetric and polar coordination environment, and when these environments are aligned, a macroscopically polar material is formed.

In addition to these "nonmagnetic" cations mentioned above, materials containing d^9 Cu^{2+} ions have been of significant interest attributable to their interesting physical properties, such as spin-gap,[33−35] magnetoresistance,[36,37] and high-Tc superconductivity.[38,39] If the magnetic phenomena are incorporated with the macroscopic polarization, magnetoelectric behavior may be observed.[40] Thus, it is of interest to investigate polar materials that incorporate Cu^{2+}. We have successfully synthesized $ACuTe_2O_7$ (A = Sr^{2+}, Ba^{2+}, or Pb^{2+}) that contains Cu^{2+}, as well as mixed valent tellurium, Te^{4+} and Te^{6+}. $BaCuTe_2O_7$ was first reported by Muller-Buschbaum et al. in 1996;[41] however, only a crystal structure was published. The structures of $SrCuTe_2O_7$ and $PbCuTe_2O_7$ are centrosymmetric (CS) and nonpolar, whereas that of $BaCuTe_2O_7$ is noncentrosymmetric (NCS) and polar. In this paper, we report on the synthesis, structure, and characterization of $ACuTe_2O_7$ (A = Sr^{2+}, Ba^{2+}, or Pb^{2+}). Attempts to synthesize $MgCuTe_2O_7$ and $CaCuTe_2O_7$ were unsuccessful, attributable to the stability of $MgTe_2O_5$,[42] $CaTe_2O_5$,[43] and Cu_3TeO_6.[44] In addition, we resynthesized polar $BaCuTe_2O_7$ and investigated its functional properties. Finally, using bond valence concepts, such as the bond strain index (BSI)[45] and global instability index (GII),[46] we describe how the "A" cation determines whether the structure is CS and nonpolar or NCS and polar.

Received: June 7, 2011
Published: July 29, 2011

EXPERIMENTAL SECTION

Reagents. $SrCO_3$ (Aldrich, 99+%), $BaCO_3$ (Aldrich, 99+%), PbO (Aldrich, 99.9+%), CuO (Fisher Scientific, 99.5+%), TeO_2 (GFS Chemicals, 99.5+%), and $H_2TeO_4 \cdot 2H_2O$ (Alfa Aesar, 99+%) were used as received.

Synthesis. Single crystals of $SrCuTe_2O_7$ and $PbCuTe_2O_7$ were grown from reaction mixtures with an excess amount of TeO_2. A 0.148 g (0.224 g) (1.00 mmol (1.00 mmol)) portion of $SrCO_3$ (PbO), 0.080 g (1.00 mmol) of CuO, and 0.798 g (5.00 mmol) of TeO_2 were placed in a platinum crucible. The crucible was gradually heated to 750 °C in air, held for 24 h, and then cooled slowly to 450 °C at a rate of 6 °C h^{-1}, followed by rapid cooling to room temperature. For $SrCuTe_2O_7$, blue plate-shaped crystals were found in ~30% yield, whereas for $PbCuTe_2O_7$, green plate-shaped crystals were recovered in ~40% yield based upon CuO.

Pure and polycrystalline $SrCuTe_2O_7$, $PbCuTe_2O_7$, and $BaCuTe_2O_7$ were prepared by conventional solid-state methods. Stoichiometric amounts of $SrCO_3$ (0.442 g, 3.00 mmol), PbO (0.671 g, 3.00 mmol), or $BaCO_3$ (0.592 g, 3.00 mmol), CuO (0.239 g, 3.00 mmol), TeO_2 (0.479 g, 3.00 mmol), and $H_2TeO_4 \cdot 2H_2O$ (0.675 g, 3.00 mmol) were thoroughly ground and pressed into pellets. The pellets were placed in alumina crucibles and heated to 650 °C (550 °C for Pb-phase) in air, held for 3 days, and then cooled to room temperature. To obtain the single phases, several intermittent grindings and refirings were essential. Purity was confirmed by powder X-ray diffraction. We also attempted to synthesize the Mg^{2+} and Ca^{2+} analogues but were unsuccessful as mixtures of MTe_2O_5 ($M = Mg^{2+}$ and Ca^{2+})[42,43] and Cu_3TeO_6[44] were found.

Single-Crystal X-ray Diffraction. A blue plate-shaped crystal ($0.02 \times 0.04 \times 0.04$ mm^3) of $SrCuTe_2O_7$ and a green plate-shaped crystal ($0.02 \times 0.03 \times 0.05$ mm^3) of $PbCuTe_2O_7$ were used for single-crystal data collection. Data were collected using a Siemens SMART diffractometer equipped with a 1K CCD area detector using graphite-monochromated Mo Kα radiation. A hemisphere of data was collected using a narrow-frame method with scan widths of 0.30° in omega and an exposure time of 40 s per frame for both $SrCuTe_2O_7$ and $PbCuTe_2O_7$. The data were integrated using the Siemens SAINT program,[47] with the intensities corrected for Lorentz, polarization, air absorption, and absorption attributable to the variation in the path length through the detector faceplate. Psi-scans for $SrCuTe_2O_7$ and $PbCuTe_2O_7$ were used for the absorption correction on the hemisphere of data. All of the data were solved by direct methods using SHELXS-97 and refined using SHELXL-97.[48,49] All of the atoms were refined with anisotropic thermal parameters and converged for $I > 2\sigma$. All calculations were performed using the WinGX-98 crystallographic software package.[50] All structural figures were drawn using the program Vesta.[51]

Powder X-ray Diffraction. Powder X-ray diffraction (PXRD) data of the materials were collected using a PANalytical X'Pert PRO diffractometer operating with Cu Kα radiation. The data were taken in the 2θ range of 5−70° in continuous scanning mode. No impurities were observed, and the calculated and experimental PXRD patterns are in excellent agreement.

Infrared (IR) Spectroscopy. Infrared spectra were recorded on a Matteson FT-IR 5000 spectrometer in the 400−4000 cm^{-1} range.

UV−vis Diffuse Reflectance Spectroscopy. UV−vis diffuse reflectance spectra were collected on a Varian Cary 500 scan UV−vis-NIR spectrophotometer over the spectral range of 200−2000 nm at room temperature. Poly(tetrafluoroethylene) was used as a reference material. Reflectance spectra were converted to absorbance with the Kubelka−Munk function.[52]

Thermogravimetric Analysis (TGA) and Differential Thermal Analysis (DTA). Thermogravimetric and differential thermal analyses were carried out on an EXSTAR TG/DTA 6300 series (SII Nano Technology Inc.). Approximately 20 mg of the samples was placed into a platinum crucible and heated and cooled between room temperature and 900 °C under nitrogen gas flowing at a rate of 10 °C min^{-1}.

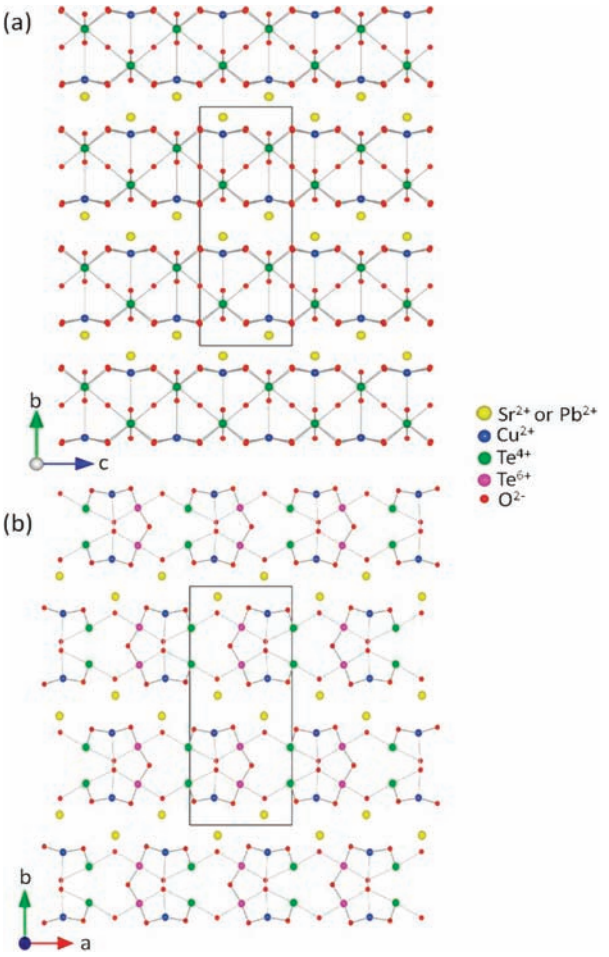

Figure 1. Ball-and-stick diagram of the $SrCuTe_2O_7$ and $PbCuTe_2O_7$ structures in the (a) *bc* and (b) *ab* planes.

Magnetic Property Measurements. Zero-field-cooled (ZFC) and field-cooled (FC) dc magnetization data were collected using a Quantum Design MPMS SQUID magnetometer using approximately 100 mg of the samples between 5 and 300 K in an applied field of 1000 Oe.

Second-Harmonic Generation. Powder SHG measurements were performed on a modified Kurtz-NLO system using a pulsed Nd:YAG laser with a wavelength of 1064 nm. A detailed description of the equipment and methodology has been published elsewhere.[5] As the powder SHG efficiency has been shown to depend strongly on particle size,[53] $BaCuTe_2O_7$ was ground and sieved into distinct particle size ranges (<20, 20−45, 45−63, 63−75, 75−90, >90 μm). Comparisons with known SHG materials were made by grinding and sieving crystalline α-SiO_2 and $LiNbO_3$ into the same particle size ranges. No index matching fluid was used in any of the experiments.

Piezoelectric Measurements. Converse piezoelectric measurements were performed using a Radiant Technologies RT66A piezoelectric test system with a TREK (model 609 × 10^{-6}) high-voltage amplifier, Precision Materials Analyzer, Precision High Voltage Interface, and an MTI 2000 Fotonic Sensor. $BaCuTe_2O_7$ was pressed into a pellet, ~1.3 cm in diameter and ~1 mm in thickness, and sintered at 650 °C for 3 days. Silver paste was applied to both sides of the pellet, and the pellet was cured at 300 °C for 12 h. The same pellet was also used in polarization measurements (see below).

dx.doi.org/10.1021/ic2012217 |*Inorg. Chem.* 2011, 50, 8663–8670

Polarization Measurements. The polarization was measured on a Radiant Technologies RT66A ferroelectric test system with a TREK high-voltage amplifier between room temperature and 215 °C in a Delta 9023 environmental test chamber. The unclamped pyroelectric coefficient, defined as dP/dT (change in polarization with respect to the change in temperature), was determined by measuring the polarization as a function of temperature. A detailed description of the methodology used has been published elsewhere.[5] To measure any possible ferroelectric behavior, the polarization was measured at room temperature under a static electric field of 13.7 kV/cm between 10 and 200 Hz. For the pyroelectric measurements, the polarization was measured statically from room temperature to 215 °C in 10 °C increments, with an electric field of 7 kV/cm. The temperature was allowed to stabilize before the polarization was measured.

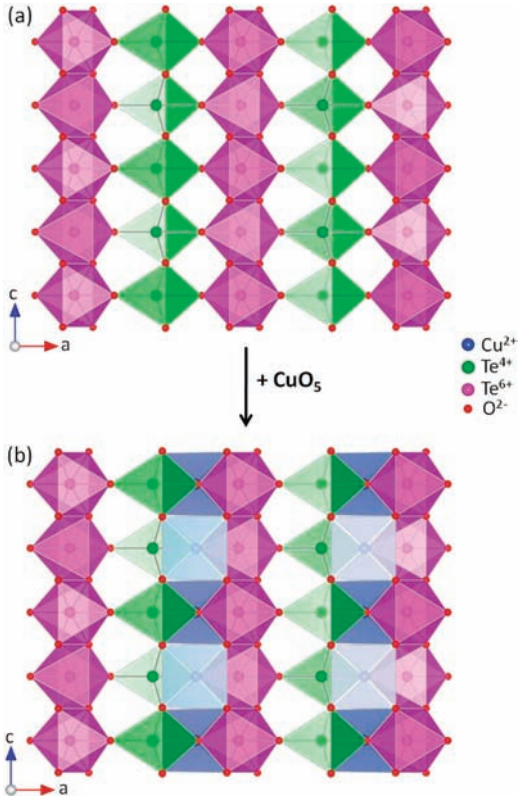

Figure 2. Polyhedral diagram of the layer in $ACuTe_2O_7$ (A = Sr^{2+}, Ba^{2+}, or Pb^{2+}) consisting of the TeO_6 and TeO_4 polyhedra (a) without and (b) with CuO_5 polyhedra.

RESULTS AND DISCUSSION

Structures. Although the reported materials have identical stoichiometries, the structures of $SrCuTe_2O_7$ and $PbCuTe_2O_7$ are different from that of $BaCuTe_2O_7$. $SrCuTe_2O_7$ and $PbCuTe_2O_7$ are isostructural with a two-dimensional crystal structure consisting of layers of corner-shared CuO_5 square pyramids, TeO_6 octahedra, and TeO_4 dispheniods (see Figure 1). The anionic $[CuTe_2O_7]^{2-}$ layers stack along the *b*-axis direction and are separated by Sr^{2+} or Pb^{2+} cations. There are two crystallographically unique tellurium sites, hereafter referred to as Te(1) and Te(2), that represent Te^{6+} and Te^{4+} in octahedral and disphenoid coordination environments, respectively. Corner-shared $Te(1)O_6$ octahedra form a one-dimensional zigzag chain along the *c*-axis, and these chains are further connected by $Te(2)O_4$ polyhedra along the *a*-axis, resulting in the two-dimensional layer (see Figure 2). The CuO_5 polyhedra alternate in the layer and are corner-shared to three $Te(1)O_6$ and three $Te(2)O_4$ polyhedra. In connectivity terms, the materials may be written as $[(CuO_{4/2}O_{1/3})^{-2.666}(Te(1)O_{5/2}O_{1/3})^{0.333}(Te(2)O_{3/2}O_{1/3})^{0.333}]^{2-}$, with the charge balance maintained by one Sr^{2+} or Pb^{2+} cation. The Cu−O bond distances in CuO_5 polyhedra range between 1.934(3) and 2.337(4) Å, attributable to first-order Jahn−Teller distortions.[54] The distances between the Cu^{2+} cations are over 4.9 Å, indicating that CuO_5 polyhedra are well separated by the $Te(1)O_6$ and $Te(2)O_4$ polyhedra. The Te(1)−O bond distances in the $Te(1)O_6$ octahedra range from 1.885(5) to 1.988(1) Å, whereas Te(2)−O bond distances in the asymmetric $Te(2)O_4$ polyhedra range between 1.833(4) and 2.205(5) Å. One of the interesting features observed in the crystal structures is the difference in the distances between the A (A = Sr^{2+}, Ba^{2+}, or Pb^{2+}) cations (see

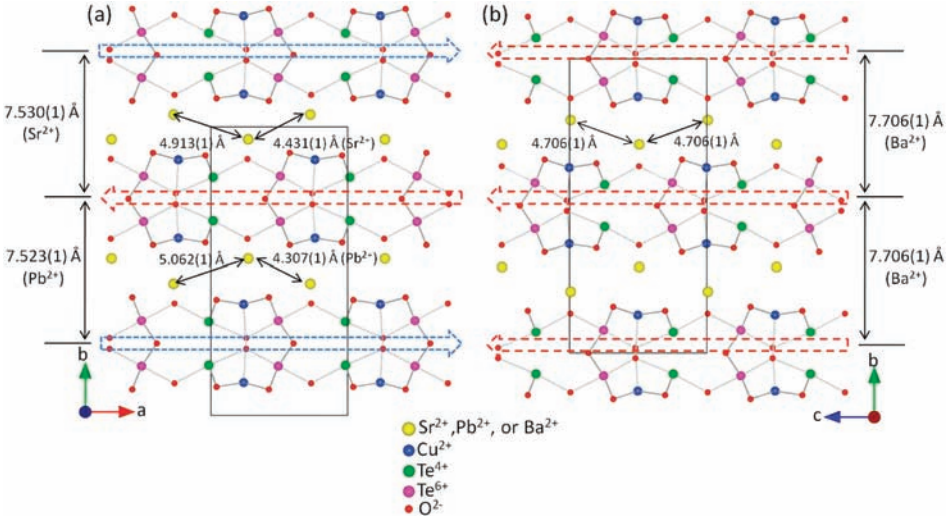

Figure 3. Ball-and-stick representation of the array of the layers in the (a) $ACuTe_2O_7$ (A = Sr^{2+} or Pb^{2+}) and (b) $BaCuTe_2O_7$. Note that the differences in the direction of the layers and the distances between the A (A = Sr^{2+}, Ba^{2+}, or Pb^{2+}) cations are found in the structures. Also, the dotted arrows indicate the direction of the dipole moment.

dx.doi.org/10.1021/ic2012217 |*Inorg. Chem.* 2011, 50, 8663–8670

Figure 3). In $SrCuTe_2O_7$ and $PbCuTe_2O_7$, there is one short and one long $Sr^{2+}-Sr^{2+}$ ($Pb^{2+}-Pb^{2+}$) distance. Short contacts of 4.431(6) Å (4.307(1)) Å) and long contacts of 4.913(7) Å (5.062(1) Å) are observed. With $BaCuTe_2O_7$, a unique $Ba^{2+}-Ba^{2+}$ distance of 4.706(1) is observed. All three A (A = Sr^{2+}, Ba^{2+}, and Pb^{2+}) cations are surrounded by 10 oxygen atoms with bond distances between 2.907(1) and 3.067(6) Å. The similar coordination environments for the A^{2+} cations indicates that the lone pair on Pb^{2+} is inert rather than stereoactive. The local coordination environments are shown in the Supporting Information, Figure S5. Bond valence calculations[55,56] resulted in values of 2.09−2.14, 5.74−5.86, 4.28−4.35, and 1.71−2.09 for Cu^{2+}, $Te(1)^{6+}$, $Te(2)^{4+}$, and alkaline earth metals and Pb^{2+} cations, respectively (see Table 4).

The local dipole moments[57,58] were calculated to examine the local polarity of the reported materials. The values shown in Table 4 are similar for each cation because the local coordination environments are very similar (see the Supporting Information, Figure S5). Also, it is found that the dipole moment of the materials is mainly attributable to the $Te(2)O_4$ polyhedra, since the $Te(2)^{4+}$ cation is in a highly asymmetric and polar coordination environment, whereas the CuO_5 and $Te(1)O_6$ polyhedra contribute less to the dipole moments attributable to their square pyramidal and nearly octahedral coordination environments, respectively. In other words, $Te(2)O_4$ polyhedra are responsible for the macroscopic polarity, if any, of the materials. However, the crystal structures of $SrCuTe_2O_7$ and $PbCuTe_2O_7$ are CS and nonpolar, whereas $BaCuTe_2O_7$ is NCS and polar. As seen in Figure 3, for the Sr^{2+} and Pb^{2+} phases, the $Te(2)O_4$ polyhedra are directed in an antiparallel manner; thus, the local polarity cancels and the macroscopic polarity is zero. For $BaCuTe_2O_7$, however, the polar units of the $Te(2)O_4$ polyhedra align in a parallel manner, resulting in macroscopic polarity. To better understand why $SrCuTe_2O_7$ and $PbCuTe_2O_7$ are CS and nonpolar, but $BaCuTe_2O_7$ is NCS and polar, we investigated what determines the alignment of the $Te(2)O_4$ polyhedra. As seen in Figure 3, although each two-dimensional layer of $[CuTe_2O_7]^{2-}$ is the same in all three materials, the A (A = Sr^{2+}, Ba^{2+}, or Pb^{2+}) cations residing between the layers are different. With respect to the A^{2+} cations, the ionic radii are 1.36, 1.40, and 1.52 Å for Sr^{2+}, Pb^{2+}, and Ba^{2+}, respectively.[59] If we replace Sr^{2+} or Pb^{2+} with the larger Ba^{2+} cation, in their CS structure, we notice that the $[CuTe_2O_7]^{2-}$ layer separation is too small. In other words, when the larger Ba^{2+} cation is introduced into the crystal structures of Sr/Pb phases, a structural strain is produced between the layers. To minimize this strain, the layers need to separate to accommodate the larger Ba^{2+} cation. This phenomenon is clearly seen in the increase of the *b*-axis of the unit cell parameters (see Table 1). The *b*-axis of $BaCuTe_2O_7$ is larger compared to those of $SrCuTe_2O_7$ and $PbCuTe_2O_7$, whereas the *a*- and the *c*-axes remain almost constant.

As seen in Figure 4, a structural strain occurs attributable to the interactions between the A (A = Sr^{2+}, Ba^{2+}, or Pb^{2+}) cations and two oxygens bonded to the $Te(1)O_6$ octahedra. The Sr(Pb)−O(4) distances are 2.652(3) (2.557(3)) and 2.656(3) (2.634(3)) Å (see Table 2). These distances seem to be relatively short compared to the larger Ba^{2+} cation as the Ba−O distances, in $BaCuTe_2O_7$, are 3.004(2) and 2.753(2) Å. In other words, for the larger Ba^{2+} cation to be introduced into the CS and nonpolar structure of the Sr/Pb phases, more space is required. However, this would be difficult, attributable to the alignment of the rigid $Te(1)O_6$ octahedra compared with the $Te(2)O_4$ units (see the

Table 1. Crystallographic Data for $SrCuTe_2O_7$, $PbCuTe_2O_7$, and $BaCuTe_2O_7$

formula	$SrCuTe_2O_7$	$PbCuTe_2O_7$	$BaCuTe_2O_7$[c]
fw	518.36	637.93	568.07
crystal system	orthorhombic	orthorhombic	orthorhombic
space group	*Pbcm* (No. 57)	*Pbcm* (No. 57)	*Ama2* (No. 40)
a (Å)	7.1464(7)	7.2033(5)	5.4869(8)
b (Å)	15.0609(15)	15.0468(10)	15.4120(8)
c (Å)	5.4380(5)	5.4691(4)	7.2066(4)
α (deg)	90	90	90
β (deg)	90	90	90
γ (deg)	90	90	90
V (Å^3)	585.30(10)	592.78(7)	609.42(10)
Z	4	4	4
R (int)	0.0548	0.0440	[d]
GOF (F^2)	1.136	1.176	[d]
$R(F)$[a]	0.0265	0.0211	0.038
$R_w(F_o^2)$[b]	0.0654	0.0519	0.072

[a] $R(F) = \Sigma||F_o| - |F_c||/\Sigma|F_o|$. [b] $R_w(F_o^2) = [\Sigma w(F_o^2 - F_c^2)^2/\Sigma w(F_o^2)^2]^{1/2}$ [c] Sedello, O.; Mueller-Buschbaum, H. *Z. Naturforsch., B: J. Chem. Sci.* **1996**, *51*, 465. [d] Not given in the original article.

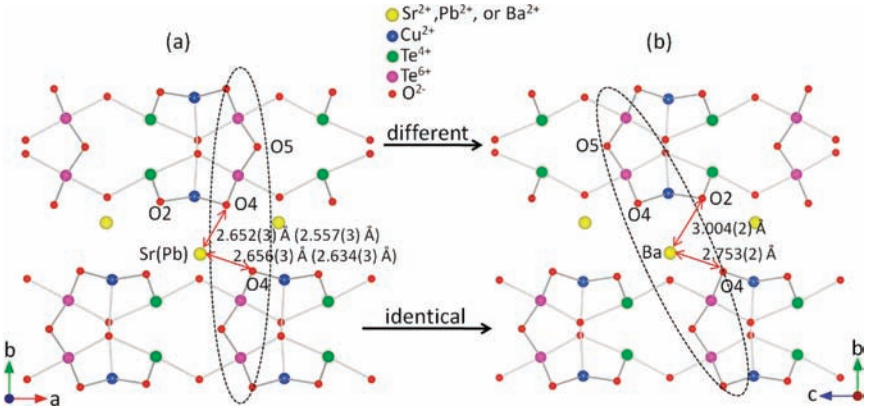

Figure 4. Ball-and-stick representation of the coordination environments of the A (A = Sr^{2+}, Ba^{2+}, or Pb^{2+}) cations in the (a) $ACuTe_2O_7$ (A = Sr^{2+} or Pb^{2+}) and (b) $BaCuTe_2O_7$. Note that the distances of the Ba−O are longer than those of the Sr(Pb)−O. Also, the alignment of the above layers are different, whereas the below layers are identical. The circled regions indicate the alignment of the $Te(1)O_6$ octahedra.

dx.doi.org/10.1021/ic2012217 |*Inorg. Chem.* 2011, 50, 8663–8670

Table 2. Selected Bond Distances (Å) for $ACuTe_2O_7$ (A = Sr^{2+}, Ba^{2+}, and Pb^{2+})

$SrCuTe_2O_7$		$PbCuTe_2O_7$		$BaCuTe_2O_7$	
Sr(1)−O(1) × 2	2.907(1)	Pb(1)−O(1) × 2	2.939(2)	Ba(1)−O(1) × 2	2.974(1)
Sr(1)−O(2) × 2	2.731(3)	Pb(1)−O(2) × 2	2.865(4)	Ba(1)−O(2) × 2	2.796(2)
Sr(1)−O(2) × 2	3.047(4)	Pb(1)−O(2) × 2	3.067(6)	Ba(1)−O(2) × 2	3.004(2)
Sr(1)−O(4) × 2	2.652(3)	Pb(1)−O(4) × 2	2.557(3)	Ba(1)−O(4) × 2	2.753(2)
Sr(1)−O(4) × 2	2.656(3)	Pb(1)−O(4) × 2	2.634(3)	Ba(1)−O(4) × 2	2.824(2)
Te(1)−O(1)	1.937(3)	Te(1)−O(1)	1.942(5)	Te(1)−O(1)	1.945(3)
Te(1)−O(3)	1.889(3)	Te(1)−O(3)	1.885(5)	Te(1)−O(3)	1.891(2)
Te(1)−O(4) × 2	1.902(3)	Te(1)−O(4) × 2	1.913(3)	Te(1)−O(4) × 2	1.906(2)
Te(1)−O(5) × 2	1.975(2)	Te(1)−O(5) × 2	1.973(2)	Te(1)−O(5) × 2	1.988(1)
Te(2)−O(1)	2.030(3)	Te(2)−O(1)	2.055(5)	Te(2)−O(1)	2.053(3)
Te(2)−O(2) × 2	1.848(3)	Te(2)−O(2) × 2	1.833(4)	Te(2)−O(2) × 2	1.848(2)
Te(2)−O(3)	2.139(3)	Te(2)−O(3)	2.205(5)	Te(2)−O(3)	2.154(2)
Cu(1)−O(2) × 2	1.949(3)	Cu(1)−O(2) × 2	1.939(4)	Cu(1)−O(2) × 2	1.969(2)
Cu(1)−O(3)	2.337(4)	Cu(1)−O(3)	2.323(5)	Cu(1)−O(3)	2.272(2)
Cu(1)−O(4) × 2	1.934(3)	Cu(1)−O(4) × 2	1.957(3)	Cu(1)−O(4) × 2	1.946(2)

Table 3. Comparison of BVS, BSI, and GII Values in Different Structures[a]

	BVS			BSI			GII		
	Sr^{2+}	Pb^{2+}	Ba^{2+}	Sr^{2+}	Pb^{2+}	Ba^{2+}	Sr^{2+}	Pb^{2+}	Ba^{2+}
$SrCuTe_2O_7$	1.72	1.75	2.70	0.073	0.075	0.074	0.185	0.182	0.255
$PbCuTe_2O_7$	1.69	1.71	2.74	0.076	0.078	0.077	0.191	0.188	0.262
$BaCuTe_2O_7$	1.36	1.33	2.13	0.075	0.081	0.074	0.281	0.289	0.190

[a] For BVS, the values for each cation in the second column were calculated in the three structures. For example, the BVS calculations of the Sr^{2+}, Pb^{2+}, and Ba^{2+} in the $SrCuTe_2O_7$ resulted in the values of 1.72, 1.75, and 2.70, respectively. Also, for BSI and GII, the same methods were used.

Table 4. BVS, BSI, and GII Values; Dipole Moments for $ACuTe_2O_7$ (A= Sr^{2+}, Ba^{2+}, and Pb^{2+}); SHG Efficiency (Relative to α-SiO_2); Piezoelectric Response (pm/V); and Pyroelectric Coefficient ($\mu C/m^2 \cdot K$ at 90 °C) for $BaCuTe_2O_7$

	BVS						dipole moments					
compounds	A^{2+}	Cu^{2+}	$Te(1)^{6+}$	$Te(2)^{4+}$	BSI	GII	Cu^{2+}	$Te(1)^{6+}$	$Te(2)^{4+}$	SHG	piezo d_{33}	pyro coeff
$SrCuTe_2O_7$	1.72	2.14	5.86	4.35	0.073	0.185	1.86	4.03	9.61			
$PbCuTe_2O_7$	1.71	2.11	5.77	4.30	0.078	0.188	1.98	3.45	9.86			
$BaCuTe_2O_7$	2.13	2.09	5.74	4.28	0.074	0.190	1.50	3.45	10.14	70	49	−9.5

circled region in Figure 4a). We feel that the $Te(1)O_6$ octahedra are more rigid compared with the $Te(2)O_4$ polyhedra, since the latter exhibits a stereoactive lone pair that provides more flexibility, that is, a greater range, of the Te−O bonds and O−Te−O angles. Thus, when the Ba^{2+} cation replaces Sr^{2+} or Pb^{2+}, the most effective way to reduce this structural strain is to remove the structural rigidity created by the alignment of the $Te(1)O_6$ polyhedra (see Figure 4b). With the presence of the Ba^{2+} cation, the alternative alignment of the $Te(1)O_6$ and $Te(2)O_4$ polyhedra provides more flexibility to the structure, resulting in overall longer distances of the Ba−O compared to those of the Sr(Pb)−O. This also results in the parallel alignment of the $Te(2)O_4$ polyhedra in each layer for $BaCuTe_2O_7$ (see Figure 3). As a result, the local dipole moments observed in the $Te(2)O_4$ polyhedra do not cancel, but are aligned in the same direction, resulting in macroscopic polarity. The bond valence sum (BVS) calculations in Table 3 support this size effect. When Ba^{2+} in $BaCuTe_2O_7$ is replaced with Sr^{2+} or Pb^{2+}, and the BVS are calculated, values of 1.36 and 1.33 are obtained, indicating substantial underbonding. Conversely, when Sr^{2+} and Pb^{2+} are replaced with Ba^{2+}, the BVS resulted in values of 2.70 and 2.74 for Sr^{2+} and Pb^{2+}, respectively, indicating substantial overbonding, whereas the BVS of the Sr^{2+} and Pb^{2+} cations remained nearly constant when interchanged. The size argument is supported by the bond strain index (BSI)[45] and global instability index (GII)[46] values. Values greater than 0.05 valence units (vu) indicate that the structure is strained, whereas values greater than 0.20 vu indicate a strain so great that the structure is unstable.[60] For all the materials, GII values are substantially greater than the BSI values, indicating that the lattice-induced strain is stronger than the electronic strain (see Table 4). This is not unexpected because only the $Te(2)^{4+}$ cation among the metal cations undergoes a SOJT distortion. To examine the size effect, we calculated BSI and GII values in the hypothetical structures, as was done with the BVS (see Table 3). When Ba^{2+} is adopted in the structure of $SrCuTe_2O_7$ or $PbCuTe_2O_7$ and vice versa, the

dx.doi.org/10.1021/ic2012217 |Inorg. Chem. 2011, 50, 8663–8670

GII values become much greater than 0.20 vu, indicating that the hypothetical structures are very unstable, whereas when Sr^{2+} and Pb^{2+} are interchanged, the values remain almost constant. Thus, it is thought that the A (A = Sr^{2+}, Ba^{2+}, or Pb^{2+}) cation size is responsible for the structural change between NCS and polar $BaCuTe_2O_7$ and CS and nonpolar $SrCuTe_2O_7$ and $PbCuTe_2O_7$.

Infrared Spectroscopy. The IR spectra of $SrCuTe_2O_7$, $BaCuTe_2O_7$, and $PbCuTe_2O_7$ reveal Cu−O and Te−O vibrations between 400 and 1000 cm^{-1}. The bands observed in the ranges of 700−810 and 600−680 cm^{-1} can be assigned to Te^{4+}−O and Te^{6+}−O stretching vibrations, and the bands occurring at 500−580 and 400−495 cm^{-1} can be attributed to Te^{6+}−O−Te^{6+} and Cu^{2+}−O vibrations, respectively.[61−64] The IR spectra and assignments are found in the Supporting Information, Figure S2.

UV−vis Diffuse Reflectance Spectroscopy. $SrCuTe_2O_7$ and $BaCuTe_2O_7$ are blue, whereas $PbCuTe_2O_7$ is green. The UV−vis spectra reveal that the absorption energy for all three compounds is approximately over 2.6 eV. Absorption (K/S) data were calculated from the Kubelka−Munk function[52]

$$F(R) = \frac{(1-R)^2}{2R} = \frac{K}{S}$$

with R representing the reflectance, K the absorption, and S the scattering. In a K/S versus E (eV) plot, extrapolating the linear part of the rising curve to zero provides the onset of absorption at 2.80, 2.67, and 2.79 eV for $SrCuTe_2O_7$, $PbCuTe_2O_7$, and $BaCuTe_2O_7$, respectively, revealing semiconducting properties of all three compounds. Also, the two peaks found in the region below 2.3 eV are attributable to the d−d transition of the Cu^{2+} cation. The UV−vis diffuse reflectance spectra for the reported materials are shown in the Supporting Information, Figure S3.

Thermal Properties. The thermal behavior of $SrCuTe_2O_7$, $BaCuTe_2O_7$, and $PbCuTe_2O_7$ was investigated using thermogravimetric analysis (TGA) and differential thermal analysis (DTA). For all of the materials, weight loss occurred attributable to vaporization of tellurium oxide. From the DTA data, it was observed that all of the materials melt incongruently. TGA data revealed that the decomposition started at approximately 660, 580, and 680 °C for $SrCuTe_2O_7$, $BaCuTe_2O_7$, and $PbCuTe_2O_7$, respectively, consistent with the DTA data. For $SrCuTe_2O_7$ and $BaCuTe_2O_7$, two main endothermic peaks found above 700 °C in the heating cycle of DTA data indicate that the starting materials decomposed to $Sr_2Te_3O_8$,[65] $SrTe_2O_5$,[66] $Ba_2Te_3O_8$,[67] $BaTe_2O_5$,[68] CuO,[69] and Cu_2O,[70] as confirmed by powder X-ray diffraction data. For $PbCuTe_2O_7$, however, several endothermic peaks are found above approximately 600 °C in the heating cycle of DTA data, and $PbCuTe_2O_7$ decomposes to PbO,[71] CuO,[69] Cu_2O,[70] and an unidentified phase, as confirmed by powder X-ray diffraction data. The exothermic peaks in the cooling cycle of DTA data are thought be attributable to recrystallization of the residues after decomposition. The diagrams of TGA and DTA are found in the Supporting Information, Figure S4.

Functional Properties: Second-Harmonic Generation, Piezoelectricity, and Polarization. As $BaCuTe_2O_7$ crystallizes in the polar noncentrosymmetric space group, *Ama*2, we investigated its SHG, piezoelectric, and polarization properties. Powder SHG measurements using 1064 nm radiation revealed an efficiency of approximately 70 × α-SiO_2 (see Figure S6 in the Supporting Information). This moderate SHG efficiency is likely attributable to the partial parallel alignment of the local dipole moments in the individual asymmetric $Te(2)O_4$ polyhedra. Although the $Te(1)^{6+}$ cation is in an octahedral coordination environment, the dipole moment associated with the $Te(1)O_6$ octahedra is small, attributable to the nearly equal Te−O bond distances. Also, it should be noted that $Te(1)^{6+}$ cations cannot undergo SOJT distortions. Additional SHG measurements indicate that $BaCuTe_2O_7$ exhibits nonphase-matching behavior (type 1) and falls into the class C category of SHG materials as defined by Kurtz and Perry.[53] The average NLO susceptibility $\langle d_{eff}\rangle_{exp}$ was determined to be ∼4.6 pm/V.[5] Converse piezoelectric measurements were also performed on $BaCuTe_2O_7$. Twenty measurements were done and averaged under a maximum voltage of 1000 V. A d_{33} piezoelectric charge constant of 49 pm/V was obtained.

Because $BaCuTe_2O_7$ is polar as well as noncentrosymmetric, polarization measurements were performed. Although polarization loops appear similar to ferroelectric hysteresis loops, the material is not ferroelectric. In other words, the macroscopic polarization cannot be switched under an external electric field. The observed polarization loops are likely attributable to dielectric loss and not ferroelectric hysteresis.[72] For a better understanding of why $BaCuTe_2O_7$ does not exhibit ferroelectric behavior, it is necessary to consider the local coordination environment and polarity of the $Te(2)O_4$ polyhedra. Recall that the $Te(2)O_4$ polyhedra are responsible for the macroscopic polarization in $BaCuTe_2O_7$. For $BaCuTe_2O_7$ to exhibit ferroelectric behavior, the local polarization of $Te(2)O_4$ polyhedra must be reversed in the presence of an external electric field. This

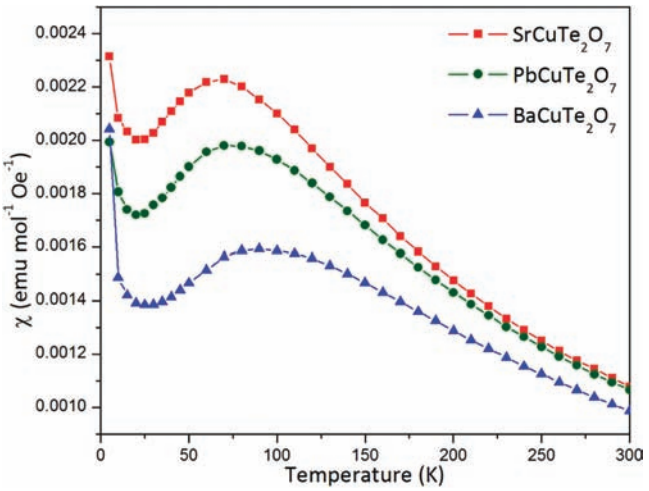

Figure 5. Magnetic susceptibilities (χ) versus temperature (K) data at a magnetic field of 1000 Oe.

Table 5. Constants Extracted from the Magnetic Susceptibility Data for $ACuTe_2O_7$ (A = Sr^{2+}, Ba^{2+}, and Pb^{2+})[a]

	C (cm^3 K mol^{-1})	Θ (K)	χ_{TIP} (emu mol^{-1} Oe^{-1})	μ_B
$SrCuTe_2O_7$	0.401(2)	−71.0(4)	$1.87(1) \times 10^{-7}$	1.80(2)
$PbCuTe_2O_7$	0.415(2)	−89.8(2)	$3.54(3) \times 10^{-6}$	1.83(2)
$BaCuTe_2O_7$	0.421(1)	−126.8(1)	$4.23(1) \times 10^{-6}$	1.84(1)

[a] C, Θ, χ_{TIP}, and μ_B represent the Curie constant, Weiss constant, temperature-independent paramagnetism term, and Bohr magneton, respectively.

dx.doi.org/10.1021/ic2012217 |*Inorg. Chem.* 2011, 50, 8663–8670

seems to be energetically very unfavorable because, for macroscopic polarization reversal, it is necessary that either the tellurium atom moves through four oxygen atoms or Te−O bonds break and reform. Although $BaCuTe_2O_7$ is not ferroelectric, the polar space group implies that the material may exhibit pyroelectric behavior. Pyroelectricity is formally defined as the temperature dependence of the spontaneous polarization with a pyroelectric coefficient $p = (\partial P_s/\partial T)$, where P_s is the spontaneous polarization and T is the temperature.[3,4] To determine the pyroelectric coefficient, p, the change in polarization as a function of temperature was measured, resulting in value of $-9.5\ \mu C\ m^{-2}\ K^{-1}$. This value is consistent with other nonferroelectric pyroelectric materials, for example, ZnO ($-9.4\ \mu C\ m^{-2}\ K^{-1}$) and tourmaline ($-4.0\ \mu C\ m^{-2}\ K^{-1}$).[4]

Magnetic Properties. The magnetic properties of all three materials, $ACuTe_2O_7$ (A = Sr^{2+}, Ba^{2+}, and Pb^{2+}), are very similar. The temperature dependence of the magnetic properties for $SrCuTe_2O_7$, $BaCuTe_2O_7$, and $PbCuTe_2O_7$ are shown in Figure 5. The susceptibility data could be fit to a modified Curie−Weiss law in the temperature range of 200−300 K with a temperature-independent paramagnetism term (TIP), $\chi = C/(T - \theta) + \chi_{TIP}$. The constants were extracted from the curve fitting and are summarized in Table 5. The effective Bohr magneton, μ_{eff}, was calculated from the Curie constant, resulting in values of 1.80(2), 1.83(2), and 1.84(1) for $SrCuTe_2O_7$, $BaCuTe_2O_7$, and $PbCuTe_2O_7$, respectively, that are in good agreement with the expected spin-only value of 1.73 μ_B/Cu^{II} ($S = 1/2$). As seen in Figure 5, the susceptibilities increase as the temperature decreases above approximately 100 K. Broad maxima are then observed at around 70, 71, and 90 K for $SrCuTe_2O_7$, $BaCuTe_2O_7$, and $PbCuTe_2O_7$, respectively, indicating that long-range magnetic ordering does not occur in the materials. The increase in the susceptibilities below approximately 25 K is thought to be attributable to paramagnetic impurities of the materials. The negative Weiss constants in Table 5 reveal that the materials exhibit antiferromagnetic interactions. This antiferromagnetic interaction could arise from a variety of nonmagnetic Cu−O−Te−O−Cu interactions, where the 5s or 5p orbital of the tellurium cation may be used for magnetic interaction. Direct magnetic interaction between the Cu^{2+} cations in the layer is negligible, attributable to their long distances of approximately 5 Å. The Cu^{2+}−Cu^{2+} interactions between the layers are also negligible since the layers are well separated by the A (A = Sr^{2+}, Pb^{2+}, or Ba^{2+}) cations with distances greater than 5 Å.

CONCLUSION

Two new quaternary oxide materials, $SrCuTe_2O_7$ and $PbCuTe_2O_7$, have been successfully synthesized and characterized. Interestingly, these materials crystallize in a centrosymmetric space group, whereas the Ba analogue, $BaCuTe_2O_7$, crystallizes in a noncentrosymmetric polar space group. Through a careful examination of the crystal structures and using bond valence concepts, it was determined that the A (A = Sr^{2+}, Ba^{2+}, or Pb^{2+}) cation size plays a crucial role concerning the centricity of the structures. For the large Ba^{2+} cation, the lattice-induced strain results in the parallel alignment of the individual polar TeO_4 polyhedra. Thus, only $BaCuTe_2O_7$ is macroscopically polar. The moderate SHG efficiency for $BaCuTe_2O_7$ is also attributable to the partial alignment of the asymmetric TeO_4 polyhedra. Although $BaCuTe_2O_7$ is polar, the frequency-dependent polarization measurements revealed that it is not ferroelectric; that is, the macroscopic polarization cannot be switched in the presence of the external electric field.

ASSOCIATED CONTENT

Supporting Information. X-ray data in CIF format, powder XRD patterns, IR and UV−vis spectra, TGA and DTA diagrams, piezoelectric and polarization loops, and detailed bond valence calculation table. This material is available free of charge via the Internet at http://pubs.acs.org.

AUTHOR INFORMATION

Corresponding Author
*E-mail: psh@uh.edu.

ACKNOWLEDGMENT

J.Y., S.-H.K., and P.S.H. thank the Robert A. Welch Foundation (Grant E-1457), the Texas Center for Superconductivity, the NSF (DMR-0652150) for support, and the Youngstown State S&CIF X-ray Facility funded by NSF Grant 0087210, Ohio Board of Regents Grant CAP-491, for the single-crystal data. J.Y. thanks the International Centre for Diffraction Data for the 2011 Ludo Frevel Crystallography Scholarship Award.

REFERENCES

(1) Auciello, O.; Scott, J. F.; Ramesh, R. *Phys. Today* **1998**, *51*, 22.
(2) Haertling, G. H. *J. Am. Ceram. Soc.* **1999**, *82*, 797.
(3) Lang, S. B.; D.-G., D. K. In *Handbook of Advanced Electronic and Photonic Materials and Devices*; Nalwa, H. S., Ed.; Academic Press: San Francisco, CA, 2001; Vol. 4, p 1.
(4) Lang, S. B. *Phys. Today* **2005**, *58*, 31.
(5) Ok, K. M.; Chi, E. O.; Halasyamani, P. S. *Chem. Soc. Rev.* **2006**, *35*, 710.
(6) Hahn, T. *International Tables for Crystallography, Vol. A, Space Group Symmetry*; Kluwer Academic: Dordrecht, Holland, 2006; Vol. A.
(7) Halasyamani, P. S.; Poeppelmeier, K. R. *Chem. Mater.* **1998**, *10*, 2753.
(8) Cooper, V. R.; Johnston, K.; Rabe, K. M. *Phys. Rev. B: Condens. Matter Mater. Phys.* **2007**, *76*, 020103.
(9) Inaguma, Y.; Yoshida, M.; Katsumata, T. *J. Am. Chem. Soc.* **2008**, *130*, 6704.
(10) Eklund, C. J.; Fennie, C. J.; Rabe, K. M. *Phys. Rev. B: Condens. Matter Mater. Phys.* **2009**, *79*, 220101.
(11) Claridge, J. B.; Hughes, H.; Bridges, C. A.; Allix, M.; Suchomel, M. R.; Niu, H.; Kuang, X.; Rosseinsky, M. J.; Bellido, N.; Grebille, D.; Perez, O.; Simon, C.; Pelloquin, D.; Blundell, S. J.; Lancaster, T.; Baker, P. J.; Pratt, F. L.; Halasyamani, P. S. *J. Am. Chem. Soc.* **2009**, *131*, 14000.
(12) Zhang, J.-H.; Hu, C.-L.; Xu, X.; Kong, F.; Mao, J.-G. *Inorg. Chem.* **2011**, *50*, 1973.
(13) Wu, X.; Rabe, K. M.; Vanderbilt, D. *Phys. Rev. B: Condens. Matter Mater. Phys.* **2011**, *83*, 020104.
(14) Wu, H.; Pan, S.; Poeppelmeier, K. R.; Li, H.; Jia, D.; Chen, Z.; Fan, X.; Yang, Y.; Rondinelli, J. M.; Luo, H. *J. Am. Chem. Soc.* **2011**, *133*, 7786.
(15) Sun, C.-F.; Hu, C.-L.; Xu, X.; Yang, B.-P.; Mao, J.-G. *J. Am. Chem. Soc.* **2011**, *133*, 5561.
(16) Nakamura, Y.; Kawai, M.; Azuma, M.; Kubota, M.; Shimada, M.; Aiba, T.; Shimakawa, Y. *Jpn. J. Appl. Phys.* **2011**, *50*, 031505.
(17) Benedek, N. A.; Fennie, C. J. *Phys. Rev. Lett.* **2011**, *106*, 107204.
(18) Zhang, W.-L.; Cheng, W.-D.; Zhang, H.; Geng, L.; Lin, C.-S.; He, Z.-Z. *J. Am. Chem. Soc.* **2010**, *132*, 1508.
(19) Yang, T.; Sun, J.; Yeon, J.; Halasyamani, P. S.; Huang, S.; Hemberger, J.; Greenblatt, M. *Chem. Mater.* **2010**, *22*, 4814.

(20) Turp, S. A.; Hargreaves, J.; Baek, J.; Halasyamani, P. S.; Hayward, M. A. *Chem. Mater.* **2010**, *22*, 5580.
(21) Sun, C.-F.; Hu, C.-L.; Xu, X.; Mao, J.-G. *Inorg. Chem.* **2010**, *49*, 9581.
(22) Kim, S.-H.; Halasyamani, P. S.; Melot, B. C.; Seshadri, R.; Green, M. A.; Sefat, A. S.; Mandrus, D. *Chem. Mater.* **2010**, *22*, 5074.
(23) Huang, Y.-Z.; Wu, L.-M.; Wu, X.-T.; Li, L.-H.; Chen, L.; Zhang, Y.-F. *J. Am. Chem. Soc.* **2010**, *132*, 12788.
(24) Chung, I.; Jang, J.-I.; Malliakas, C. D.; Ketterson, J. B.; Kanatzidis, M. G. *J. Am. Chem. Soc.* **2010**, *132*, 384.
(25) Bera, T. K.; Jang, J. I.; Song, J.-H.; Malliakas, C. D.; Freeman, A. J.; Ketterson, J. B.; Kanatzidis, M. G. *J. Am. Chem. Soc.* **2010**, *132*, 3484.
(26) Opik, U.; Pryce, M. H. L. *Proc. R. Soc. London, Ser. A* **1957**, *238*, 425.
(27) Bader, R. F. W. *Mol. Phys.* **1960**, *3*, 137.
(28) Bader, R. F. W. *Can. J. Chem.* **1962**, *40*, 2140.
(29) Pearson, R. G. *J. Am. Chem. Soc.* **1969**, *91*, 4947.
(30) Pearson, R. G. *THEOCHEM* **1983**, *12*, 25.
(31) Wheeler, R. A.; Whangbo, M. H.; Hughbanks, T.; Hoffmann, R.; Burdett, J. K.; Albright, T. A. *J. Am. Chem. Soc.* **1986**, *108*, 2222.
(32) Goodenough, J. B. *Annu. Rev. Mater. Sci.* **1998**, *28*, 1.
(33) Cepas, O.; Kakurai, K.; Regnault, L. P.; Ziman, T.; Boucher, J. P.; Aso, N.; Nishi, M.; Kageyama, H.; Ueda, Y. *Phys. Rev. Lett.* **2001**, *87*, 167205.
(34) Kodama, K.; Takigawa, M.; Horvatic, M.; Berthier, C.; Kageyama, H.; Ueda, Y.; Miyahara, S.; Becca, F.; Mila, F. *Science* **2002**, *298*, 395.
(35) Xu, J.; Assoud, A.; Soheilnia, N.; Derakhshan, S.; Cuthbert, H. L.; Greedan, J. E.; Whangbo, M. H.; Kleinke, H. *Inorg. Chem.* **2005**, *44*, 5042.
(36) Zeng, Z.; Greenblatt, M.; Subramanian, M. A.; Croft, M. *Phys. Rev. Lett.* **1999**, *82*, 3164.
(37) Sanchez-Benitez, J.; Prieto, C.; de Andres, A.; Alonso, J. A.; Martinez-Lope, M. J.; Casais, M. T. *Phys. Rev. B: Condens. Matter Mater. Phys.* **2004**, *70*, 024419.
(38) Schneemeyer, L. F.; Waszczak, J. V.; Siegrist, T.; Van Dover, R. B.; Rupp, L. W.; Batlogg, B.; Cava, R. J.; Murphy, D. W. *Nature* **1987**, *328*, 601.
(39) Vershinin, M.; Misra, S.; Ono, S.; Abe, Y.; Ando, Y.; Yazdani, A. *Science* **2004**, *303*, 1995.
(40) Kumar, A.; Martin, L. W.; Denev, S.; Kortright, J. B.; Suzuki, Y.; Ramesh, R.; Gopalan, V. *Phys. Rev. B: Condens. Matter Mater. Phys.* **2007**, *75*, 060101.
(41) Sedello, O.; Mueller-Buschbaum, H. *Z. Naturforsch., B: J. Chem. Sci.* **1996**, *51*, 465.
(42) Weil, M. *Acta Crystallogr., Sect. E: Struct. Rep. Online* **2005**, *E61*, i237.
(43) Troemel, M.; Ziethen-Reichnach, H. *Z. Anorg. Allg. Chem.* **1970**, *378*, 232.
(44) Falck, L.; Lindqvist, O.; Moret, J. *Acta Crystallogr., Sect. B* **1978**, *B34*, 896.
(45) Preiser, C.; Losel, J.; Brown, I. D.; Kunz, M.; Skowron, A. *Acta Crystallogr., Sect. B: Struct. Sci.* **1999**, *B55*, 698.
(46) Salinas-Sanchez, A.; Garcia-Munoz, J. L.; Rodriguez-Carvajal, J.; Saez-Puche, R.; Martinez, J. L. *J. Solid State Chem.* **1992**, *100*, 201.
(47) *SAINT Program for Area Detector Absorption Correction*, version 4.05; Siemens Analytical X-ray Systems: Madison, WI, 1995.
(48) Sheldrick, G. M. *SHELXS-97: A Program for Crystal Structure Refinement*; University of Goettingen: Goettingen, Germany, 1997.
(49) Sheldrick, G. M. *Shelxs-97: A Program for Automatic Solution of Crystal Structures*; University of Goettingen: Goettingen, Germany, 1997.
(50) Farrugia, L. J. *J. Appl. Crystallogr.* **1999**, *32*, 837.
(51) Momma, K.; Izumi, F. *J. Appl. Crystallogr.* **2008**, *41*, 653.
(52) Kubelka, P.; Munk, F. Z. *Tech. Phys.* **1931**, *12*, 593.
(53) Kurtz, S. K.; Perry, T. T. *J. Appl. Phys.* **1968**, *39*, 3798.
(54) Jahn, H. A.; Teller, E. *Proc. R. Soc. London, Ser. A* **1937**, *161*, 220.
(55) Brown, I. D.; Altermatt, D. *Acta Crystallogr., Sect. B* **1985**, *B41*, 244.
(56) Brese, N. E.; O'Keeffe, M. *Acta Crystallogr., Sect. B* **1991**, *B47*, 192.
(57) Debye, P. *Polar Molecules*; Chemical Catalog Company, Inc.: New York, 1929.
(58) Debye, P. *Phys. Z.* **1921**, *22*, 302.
(59) Shannon, R. D.; Prewitt, C. T. *Acta Crystallogr., Sect. B* **1970**, *26*, 1046.
(60) Brown, I. D. *The Chemical Bond in Inorganic Chemistry*; Oxford University Press: New York, 2002; Vol. 12.
(61) Kim, J.-H.; Halasyamani, P. S. *J. Solid State Chem.* **2008**, *181*, 2108.
(62) Pan, S.; Watkins, B.; Smit, J. P.; Marvel, M. R.; Saratovsky, I.; Poeppelmeier, K. R. *Inorg. Chem.* **2007**, *46*, 3851.
(63) Minimol, M. P.; Vidyasagar, K. *Inorg. Chem.* **2005**, *44*, 9369.
(64) Porter, Y.; Halasyamani, P. S. *Inorg. Chem.* **2003**, *42*, 205.
(65) Elerman, Y.; Kocak, M. *J. Appl. Crystallogr.* **1986**, *19*, 410.
(66) Redman, M. J.; Chen, J. H.; Binnie, W. P.; Mallio, W. J. *J. Am. Ceram. Soc.* **1970**, *53*, 645.
(67) Agarwal, R.; Singh, Z. *J. Alloys Compd.* **2006**, *414*, 230.
(68) Pashinkin, A. S. *Izv. Akad. Nauk SSSR, Neorg. Mater.* **1975**, *11*, 1650.
(69) Asbrink, S.; Norrby, L. J. *Acta Crystallogr., Sect. B* **1970**, *26*, 8.
(70) Niggli, P. *Z. Kristallogr.* **1922**, *57*, 253.
(71) Kay, M. I. *Acta Crystallogr.* **1961**, *14*, 80.
(72) Scott, J. F. *J. Phys.: Condens. Matter* **2008**, *20*, 021001.